Solidification kinetics in SiGe alloys

Qiuming Yu*
School of Chemical Engineering, Cornell University, Ithaca, New York 14853

Michael O. Thompson
Department of Materials Science and Engineering, Cornell University, Ithaca, New York 14853

Paulette Clancy†
School of Chemical Engineering, Cornell University, Ithaca, New York 14853
(Received 8 May 1995; revised manuscript received 15 November 1995)

The solidification kinetics of SiGe alloys, modeled by the Stillinger-Weber potential, are investigated using nonequilibrium molecular-dynamics computer simulation techniques. Interface response functions and solute redistribution at the regrowing solid/liquid interface are investigated. The maximum crystallization velocity of SiGe alloys is found to decrease below the pure component values, in agreement with the results of explosive crystallization measurements. The results of solidification velocity versus interface temperature (i.e., one of the interface response functions) obtained from the simulation for SiGe alloys compare well, in most cases, with Aziz's continuous growth model assuming short-range diffusion-limited growth. Mutual trapping of Si in Ge and Ge in Si is found in both Si-rich and Ge-rich alloys, in agreement with Aziz's solute trapping theory and with experiment.

I. INTRODUCTION

During rapid solidification of a binary alloy, induced by pulsed-laser melting, the crystallization velocity is not only governed by the undercooling of the solid-liquid interface with respect to the congruent melting temperature of the alloy, i.e., as described by the interface velocity-temperature response function, but also by the solute redistribution at the solid-liquid interface. To completely determine the interface motion of solidification of a binary alloy, two interface response functions are required, one to relate interface temperature T_i and interface velocity v and one to relate the solute partitioning k_B at the solid-liquid interface to the interface velocity v. A number of theoretical models[1–3] have been developed to describe the growth kinetics of such interface-mediated phase transitions.

During solidification of single-component melts, the growth velocity is typically expressed as the product of a factor involving the thermodynamic driving force for solidification and a kinetic factor involving the interface mobility

$$v(T_i)=v_0(T_i)\left[1-\exp\left(\frac{\Delta\mu}{RT_i}\right)\right], \tag{1}$$

where T_i is the interface temperature, $v_0(T_i)$, a kinetic prefactor, the maximum speed of solidification at infinite driving force, R, the gas constant and, for pure elements, $\Delta\mu$, the Gibbs free energy change on solidification (defined to be negative for solidification). The kinetic prefactor can be described in two fundamentally different theories, the short-range diffusion-limited and collision-limited theories.

In the short-range diffusion-limited theory,[4–6] it is assumed that the rate at which atoms can move across the interface to join the solid depends, among other factors, on the mobility of atoms in the liquid. Consequently, the kinetic prefactor $v_0(T_i)$ is expressed as

$$v_0(T_i)=fdD/\lambda^2, \tag{2}$$

where D is the diffusion coefficient of the liquid, λ is the mean free path in the liquid, (D/λ^2 is the mean jump frequency), d is an average distance over which the interface moves for a successful jump, and f is the fraction of active sites at the interface ($f\leqslant 1$). This expression was modified by Jackson to include an additional entropy factor, $\exp(-\Delta S/k)$, where ΔS is the difference in entropy of the liquid and solid phases.[7] The short-range diffusion-limited theory successfully described the interface response function for silicon with the data obtained from the epitaxial explosive crystallization of amorphous Si combined with numerical temperature calculations[8] and molecular-dynamics (MD) simulation of Stillinger-Weber (SW) Si.[9]

In contrast, in the collision-limited growth model,[10] solidification potentially occurs with every impingement event from the liquid and

$$v_0(T_i)=cv_s, \tag{3}$$

where v_s is the speed of sound in the liquid and c is a numerical factor of order unity. For c-Si, v_s is approximately 8300 m/s,[11] while the dD/λ^2 of Si in the liquid at melting temperature is of the order of 150 m/s. Therefore, the crystallization events in the collision-limited growth model are expected to be more rapid than diffusive events. Stolk *et al.* found that the collision-limited growth model could not reproduce the experimental data of epitaxial explosive crystallization of amorphous silicon if the maximum interface velocity is taken to be limited by the sound velocity.[8] Aziz and Kaplan[1] have extended the relation of the growth velocity and the interface temperature for one-component materials

[Eq. (1)] to alloys by assuming that a modified free energy difference responsible for interface motion enters into Eq. (1) in the same way as that $\Delta\mu$ does for pure materials. In the version of the continuous growth model (CGM) ''without solute drag,'' this modified free-energy difference is ΔG_{DF}, the ''driving free energy'' for the transformation, which represents the entire free energy dissipated at the interface,

$$\Delta G_{\mathrm{DF}} = X_s \Delta\mu_B + (1 - X_s)\Delta\mu_A \tag{4}$$

with X_s the solute mole fraction in the solid at the interface, and $\Delta\mu_B$ and $\Delta\mu_A$ the changes in chemical potential on solidification for solute and solvent, respectively. In the CGM ''with solute drag,'' part of the overall driving free energy, ΔG_D, is consumed in driving the solute-solvent redistribution reaction and is therefore unavailable to drive interface motion. The modified energy difference is replaced by $\Delta G_C = \Delta G_{\mathrm{DF}} - \Delta G_D$. In sharp-interface models, ΔG_D is determined using the thermodynamics of irreversible processes and

$$\Delta G_C = X_l \Delta\mu_B + (1 - X_l)\Delta\mu_A \tag{5}$$

with X_l the solute mole fraction in the liquid at the interface. In a recent version of CGM,[12] ''partial-solute-drag'' is incorporated by interpolating between versions of the CGM that either include or exclude solute drag. A ''drag'' parameter β is defined as zero for the model without solute drag and unity for the model with solute drag. Eckler *et al.*[13] postulated that β varies with interface velocity.

The original CGM also proposes an expression for the solute partition coefficient, k_B, varying with growth velocity. In the CGM of Aziz and Kaplan,[1] the solidification reactions are expressed as one of complete dependence, where the solute and solvent atoms are imagined to crystallize as a hypothetical complex of solute and solvent. The interface velocity dependence of solute partitioning for dilute solutions is given by

$$k_B(v) = \frac{k_e + v/v_D}{1 + v/v_D}, \tag{6}$$

where v is the interface velocity, v_D is the diffusive velocity, and k_e is the equilibrium solute partition coefficient which can be obtained from the phase diagram.

In the past decade, most of the work on interface kinetics in rapid solidification for alloys has concentrated on the interface velocity dependence of solute partitioning for dilute alloys (i.e., the k-v relationship). The partitioning in metals[14] as well as semiconductors[14–17] was measured and found to be well described by the CGM.

The CGM predicts that if there is significant trapping of component B in a second component A, then there should be significant trapping of A in B at a similar velocity. In such cases, the partition coefficients for both alloys are equal to one. In contrast, in the model of Jackson, Gilmer, and Leamy,[2,3] the barriers to solidification for host and impurity atoms are treated independently and the fluxes of two species are summed to find the crystal growth rate. There is an upper limit to the partition coefficient which occurs at the maximum allowed velocity. Therefore the model of Jackson *et al.* does not allow the mutual trapping of A in B and of B in A. Measurements of the partition coefficient of Ge in Si and Si in Ge under rapid solidification conditions showed mutual trapping in SiGe alloys, which supports the CGM.[16]

While k-v data are relatively straightforward to measure, obtaining the v-T interface response function is an experimental challenge. Technical difficulties in measuring the interface temperature during rapid solidification have lead to relatively little work being done to determine the interface velocity-undercooling function even for single-component materials.

Recently, however, a new technique has been developed to measure the temperatures and velocities simultaneously with nanosecond resolution. This method has been used during rapid solidification of Si-As alloys induced by pulsed-laser melting, to determine the velocity-temperature interface function for alloys in the regime of complete solute trapping[18] and the regime of partial solute trapping.[17] The results are in good agreement with predictions of the CGM ''without solute drag,'' but are inconsistent with the model including the solute drag model.[17] Aziz and Boettinger[12] developed analytical expressions for the velocity-undercooling function for a planar interface during dilute alloy solidification, using Turnbull's collision-limited growth model[10] and the CGM both with and without solute trapping.[1] Comparison of the results of the analytical expressions to the numerical solutions of the nondilute kinetics model for Al-Be alloys shows that the dilute approximation breaks down at melt compositions on the order of 10 at. %.

In this paper, we report the production of an interface velocity-temperature response function for an alloy using nonequilibrium molecular-dynamics simulations. This response function was determined for SiGe alloys over a wide range of Ge compositions and undercoolings. The simulation results are then compared with the CGM. The temperature dependence of the liquid diffusion coefficients for SiGe alloys are calculated and the short-range diffusion-limited growth model is assumed for the kinetic prefactor. Mutual trapping phenomena are studied for the rapid solidification of Si-rich and Ge-rich alloys.

II. POTENTIAL MODEL AND SIMULATION METHOD

The Stillinger-Weber potential model[20] was used in this paper to represent the interactions between Si-Si, Ge-Ge, and Si-Ge. The choice of parameters for Ge-Ge and Si-Ge interactions as well as a justification of the use of empirical models for these systems were described in Refs. 21 and 22. Here, the size and energy parameters for Ge were chosen as those representing the best fit to the lattice constant and melting temperature, respectively. The other parameters in the SW potential for Ge were kept at the same values as those for Si. For the unlike Si-Ge interactions, we employed the customary Lorentz-Berthelot mixing rules. Thus, the ratios of size and energy parameters for Ge and Si were 1.04 and 0.71, respectively.

A nonequilibrium molecular-dynamics (NEMD) method[23] was used to simulate the rapid solidification of SiGe alloys induced by pulsed-laser melting. First, appropriate densities of SiGe alloys of different composition were determined at chosen substrate temperatures and zero pressure using an isobaric-isothermal NPT molecular-dynamics program. Then a constant-volume and constant-temperature (i.e., NVT)

simulation was used to equilibrate the alloy system with a solid-vapor interface at the top and a fixed lattice at the bottom. The system was heated by subjecting it to a beam of energy carriers using the method described in Ref. 23. The intensity of the beam was Gaussian in time, with a pulse duration of 15 ps and a fluence appropriate for different compositional alloys and substrate temperatures. The crystal orientation was (100) for all SiGe alloys. The simulation cell was 5×5 unit cells in the lateral directions (X and Y) and 10 unit cells in the vertical direction (Z), so that there was a longer distance for solidification to take place and better statistics can be obtained. Larger systems with $7\times7\times14$ unit cells in X, Y, and Z directions were used in some simulations to test the size effect of the simulation cell used. A bulk alloy simulation cell was used to eliminate the strain effect on solute partitioning and solidification velocity in AB/A heterostructures, which was observed in MD simulations for Lennard-Jones (LJ) alloys[24] and SiGe alloys[21] as well as in experiments.[25] Four atomic layers of atoms at the bottom of the simulation cell were fixed at their lattice positions to emulate the semi-infinite structure. Another five atomic layers of atoms on top of it were assigned as a heat bath, in which the temperature was kept constant by scaling the velocity of each atom every 30 time steps. The interface growth rate was controlled by choosing the heat bath temperature, i.e., the substrate temperature.

The positions of the atoms were separated into ''layers,'' as described in Ref. 24 for property calculation. The location of the solid-liquid interface was determined by observing the diffusion coefficients via mean-square displacement data, the two-dimensional structure factor, $S^2(k)$ (described in Ref. 24), the three-body potential energy, and the fraction of solid atoms in each layer. The solid-liquid interface for the (100) SiGe alloys were found to be 4–5 atomic layers thick.[21] The position of the interface was determined by taking an average of the heights of the last solidlike layer and of the first liquidlike layer. The interface temperature was also calculated as the average of that in these 4–5 layers.

Since the solid-liquid interface during regrowth on (100) is rough, with (111) facets, a criterion was used to determine the exact location of solidlike and liquidlike atoms at the interface without any constraint on the shape of the interface. A solidlike atom was defined as an atom with four neighbors within a distance between that for first-nearest and second-nearest neighbors in a perfect crystal and having a three-body potential energy, $U_3^*\leqslant0.21$.[26] Atoms that do not satisfy both of these requirements were considered liquidlike. Any solidlike atom with a liquidlike neighbor was taken as lying in the liquid-solid interface. Thus the partition coefficients at the interface were calculated as $X^s_{\mathrm{Ge}}/X^l_{\mathrm{Ge}}$ for Ge as an ''impurity'' in a Si-rich alloy and $X^s_{\mathrm{Si}}/X^l_{\mathrm{Si}}$ for Si as an ''impurity'' in a Ge-rich alloy. Atoms belonging to an amorphous phase are identified through determination of structure factors and diffusion coefficients, since such atoms show solidlike diffusion coefficients yet little short-range order.

III. RESULTS

A. Mutual trapping

Simulations of rapid melting and solidification of each alloy were performed at various substrate temperatures to obtain different solidification velocities. The location of the solid-liquid interface during melting and resolidification was monitored by the fraction of solidlike atoms in each layer, as described in Sec. II. The melt depth and interface temperature as a function of time for a 25 at. % Ge alloy at a substrate temperature of 1010 K, for example, are shown in Fig. 1. Each system was exposed to a 15 ps ''laser beam'' with a different energy density for different alloys and different substrate temperatures designed to melt approximately the same amount of solid in all cases. The solid alloy melts rapidly as the laser beam impinged on it, penetrating further after the laser pulse was turned off, due to the high interface temperature. As the energy was withdrawn from the system by the heat conducted into the heat bath, the interface temperature cooled and solidification occurred. As shown in Fig. 1, a steady-state regrowth was reached where the slope of the melt depth versus time, the solidification velocity, was constant and the interface temperature fluctuated around a mean value. The solidification velocity was 9.5 m/s and the interface temperature was 1098 ± 25 K at steady state for this 25 at. % Ge alloy. In contrast to simulations of regrowth in metals[27] and in LJ alloys,[24] the solid-liquid interface of SW SiGe alloys moved very smoothly and the undercooling of the interface was very well behaved during solidification, as shown in Fig. 1. Redistribution of Ge at a rapidly moving

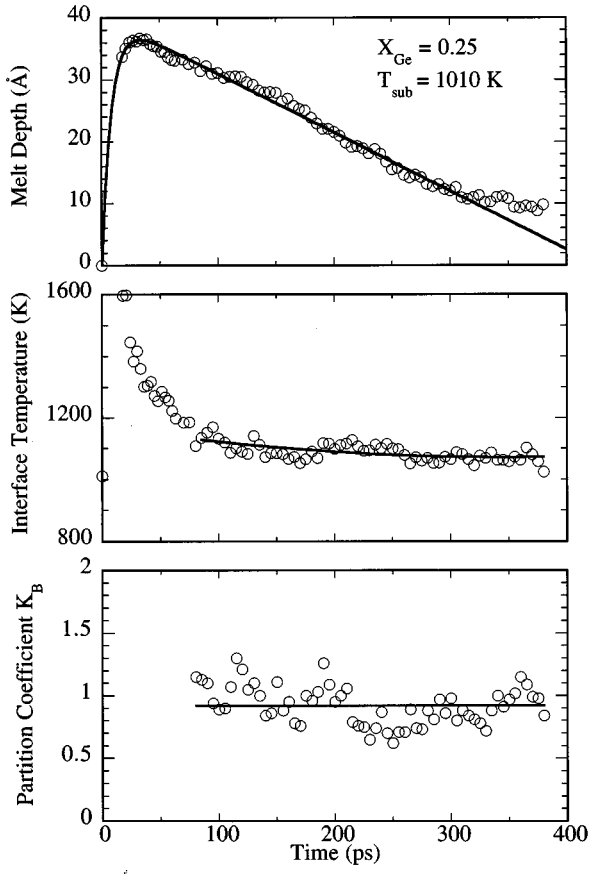

FIG. 1. Histories of the melt depth, interface temperature, and partition coefficient k_B of a nonequilibrium molecular-dynamics simulation of melting and rapid solidification for a $Si_{75}Ge_{25}$ alloy at a substrate temperature of 1010 K. Circles indicate raw data; lines represent the best fit to the data.

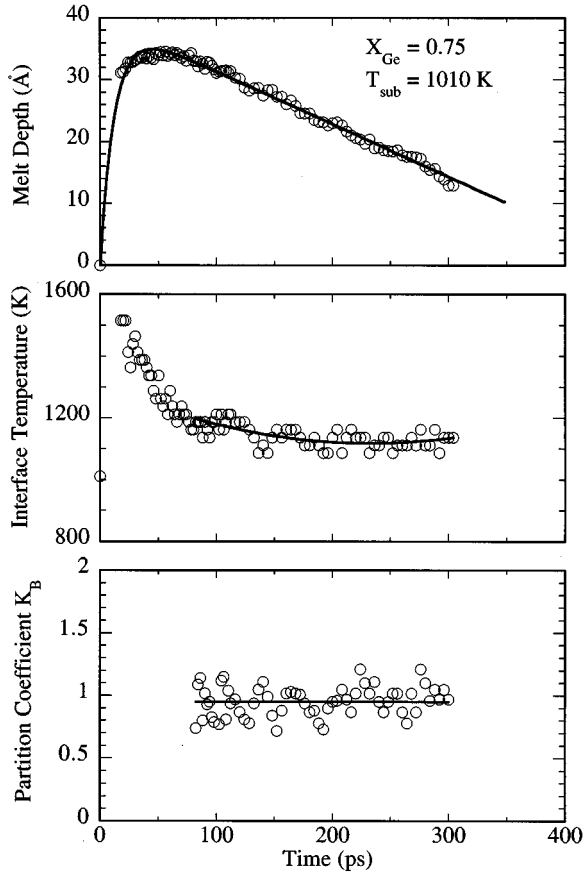

FIG. 2. Histories of the melt depth, interface temperature and partition coefficient k_B of a nonequilibrium molecular-dynamics simulation of melting and rapid solidification for a $Si_{25}Ge_{75}$ alloy at a substrate temperature of 1010 K. Key as for Fig. 1.

solid-liquid interface was studied through determinations of the partition coefficient $k_B = X^s_{Ge}/X^l_{Ge}$ at the interface, as described in Sec. II. As shown in Fig. 1, the mean value of the partition coefficient was 0.92 ± 0.15, showing significant trapping of Ge in Si at this regrowth rate. In comparison, CGM theory, using Eq. (6), gives a value of 0.90, with values of $v_D = 2$ m/s and $k_e = 0.45$.[21]

To study mutual trapping phenomena, we also performed simulations for a 25 at. % Si alloy at similar regrowth velocities (8–9 m/s). The partition coefficient here was calculated as the ratio of Si concentration in the solid at the solid-liquid interface to that in the liquid at the solid-liquid interface and indicated as k_A. The melt depth, interface temperature, and partition coefficient k_A are plotted in Fig. 2. Again, there was significant trapping; this time, trapping of Si in Ge. Comparison of the partitioning behavior of the two alloys (25 at. % Ge and 25 at. % Si) is made in Table I where it can be seen that the simulations predict mutual trapping of Si in Ge and Ge in Si in accord with experiment.[16] Aziz *et al.* performed experiments to determine the partition coefficient for Ge as an ''impurity'' in Si and for Si as an ''impurity'' in Ge.[16] Using an experimental value for v_D of roughly 1 m/s and $k_e^{Si} = 6$ from the equilibrium phase diagram, the authors used CGM theory to estimate $k_{Si} = 1.10$ at a velocity of 4 m/s (in comparison to a v_D of 2 m/s for Ge in Si). The reduced diffusive speed of Si in Ge (around 1 m/s) compared to 2 m/s for Ge in Si, is due to a lower interface temperature on the Ge-rich side of the phase diagram. Using the same values of k_e^{Si} and v_D as Aziz *et al.*, the CGM predicts that $k_A = 1.05$ at a solidification velocity of 8.5 m/s.

TABLE I. Mutual trapping of Ge as an impurity in Si and that of Si as an impurity in Ge. Results from NEMD simulations are compared with CGM theory using Eq. (6) with $v_D = 2$ m/s and $k_e = 0.45$ for Si-rich alloys and with $v_D = 0.08$ m/s and $k_e^{Si} = 6$ for Ge-rich alloys.

X_{Ge}	v (m/s)	k_{NEMD}	k_{CGM}
0.05	17.1	0.80 ± 0.23	0.94
0.25	9.5	0.92 ± 0.15	0.90
0.75	8.5	0.93 ± 0.13	1.05
0.95	9.5	0.98 ± 0.38	1.04

Table I also shows that mutual trapping phenomena occur at other Ge compositions, as evidenced by the results for 5 at. % Ge and 5 at. % Si alloys. Although there are only small amounts of solute atoms in these systems, leading to statistical uncertainties, the partition coefficients were observed to oscillate about unity at large solidification velocities for both alloys.

B. Relationship of solidification velocity and interface temperature

For single-component materials, the rate of solidification is determined by the undercooling of the interface. This interfacial undercooling is determined by achieving a balance between a heat flow due to conduction into the substrate and an enthalpy release at the interface. The interface response function relating the solidification velocity and interface temperature for crystallization of liquid Si was studied experimentally using epitaxial explosive crystallization of amorphous Si (Ref. 8) and computationally in MD simulations.[9] The experimental measurements together with numerical temperature calculations indicate that the maximum crystallization velocity for ⟨100⟩ Si is 15.8 m/s at a large undercooling of >130 K below the equilibrium melting temperature.[8] MD simulations of ⟨100⟩ Si using the SW potential show that the maximum crystallization rate is 18 m/s at an interface temperature of 1409 K, which represents an undercooling of 282 K.

There are few measurements of the interface temperature and solidification velocity for binary alloys, but this information is accessible using nonequilibrium MD simulations. As described in Sec. II, the interface temperature was calculated during solidification and the solidification velocity was obtained from the slope of the melt depth versus time curve starting from the maximum melt depth. The melt depth and solidification velocity as well as the interface temperature and solidification velocity versus time at three different substrate temperatures for 75 at. % Ge alloys are shown in Figs. 3 and 4, respectively. At higher substrate temperatures, such as 1086 and 1010 K in Figs. 3 and 4, each simulated solidification process can be divided as two regions, transient and steady-state regions. The transient region started from the maximum melt depth, where the solidification velocity is zero, and ended at the steady-state regrowth regime. During

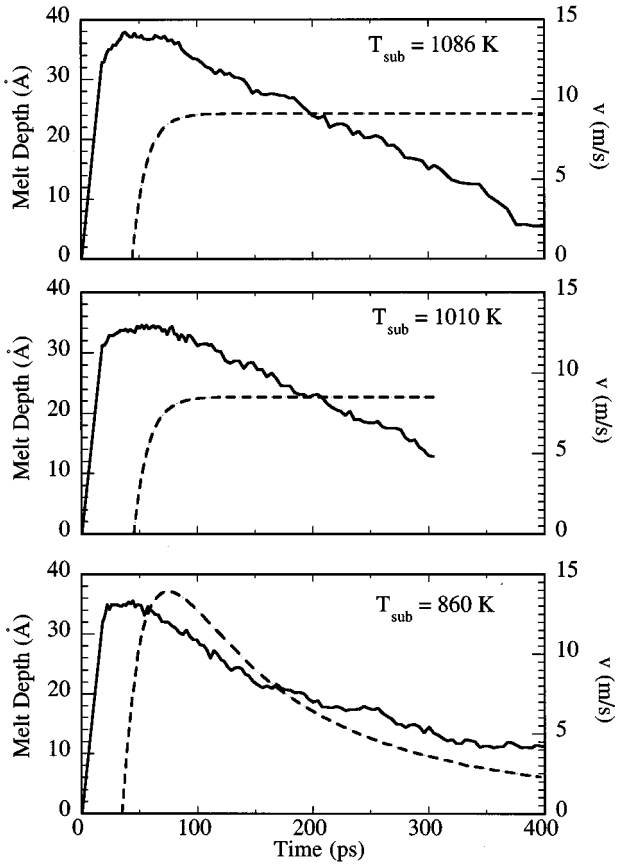

FIG. 3. The melt depth (solid line) and interface velocity (dashed line) as a function of time for a $Si_{25}Ge_{75}$ alloy at three different substrate temperatures.

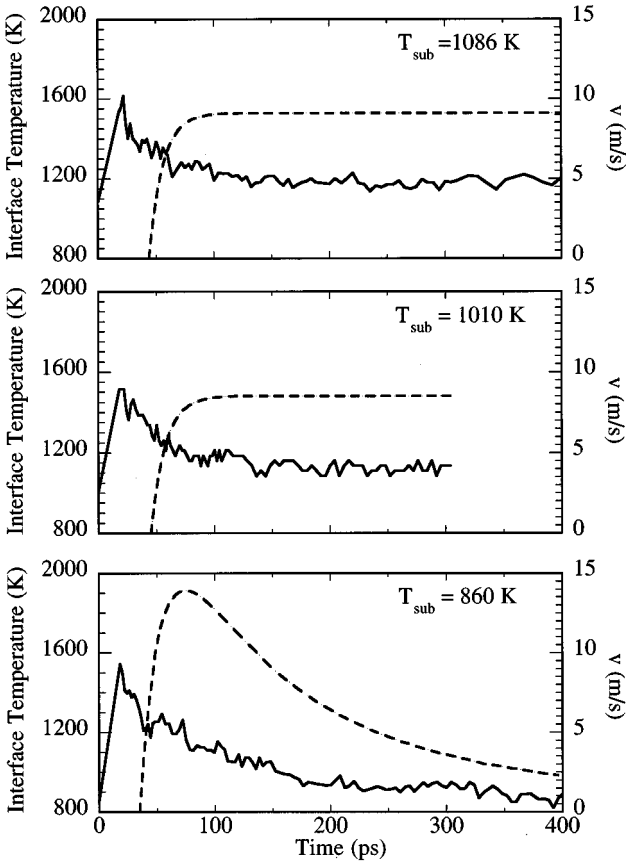

FIG. 4. The interface temperature (solid line) and interface velocity (dashed line) as a function of time for a $Si_{25}Ge_{75}$ alloy at three different substrate temperatures.

this transient region, the temperature decreased continuously. In the steady-state region, the liquid solidified at a constant velocity with a constant interface temperature. However, if the substrate temperature is very low, e.g., 860 K in Figs. 3 and 4, it is apparent from the data that steady state is not achieved during the solidification. The solidification velocity was initially very fast but slowed as the interface temperature continued to cool. When the solidification finished and the interface temperature dropped to the same value as the substrate temperature, no enthalpy was released at the solid-liquid interface and heat conduction to the substrate continued until the interface temperature fell to the substrate temperature.

In order to determine the undercooling of the interface, the congruent melting temperature T_0 of the alloy must be known. The congruent melting temperatures of SiGe alloys have been calculated by Thompson *et al.*[25] and show an almost linear relationship between the congruent melting temperature and alloy composition if partitionless melting and solidification and regular solution behavior are assumed. From these calculations, the congruent melting temperature for a 75 at. % Ge alloy is 1329 K. The interface temperatures at steady state are 1131 ± 14 K and 1137 ± 19 K, for substrate temperatures of 1086 K and 1010 K, respectively, corresponding to undercoolings of around 192–198 K. Thus, these solidifications take place on the ''front side'' of the interface response function (i.e., $T_{v,\max}>T_i>T_0$). For a substrate temperature of 860 K, the undercooling is approximately 470 K. Yater studied different mechanisms for the amorphization of crystal Si and proposed that once the interface temperature falls below the melting temperature of amorphous Si, the phase transition to a-Si is thermodynamically feasible and spontaneous nucleation may occur.[28] One possible amorphization mechanism may involve a glass transition in Si.[28]

A glass transition in Si, although as yet unseen experimentally, is speculated to occur with sufficiently large supercooling.[29] Evans and Stiffler, analyzing homogeneous nucleation data for liquid Si, have suggested that liquid Si would undergo a glass transition at a temperature of approximately 950 K.[30] Although this temperature is sufficiently low that it has not yet been observed experimentally, Horsfield and Clancy[31] found that a glassy material was produced at $\sim$1000 K at fast quench rates ($\sim10^{12}$ K/s) in MD simulations using tight-binding models for Si. Similar values of the glass transition temperature for Si were also found in the simulations using classical potentials.[32,33] The glass formation is also characterized by a convex curvature of the logarithm of the liquid diffusion coefficient versus reciprocal temperature, which will be discussed in Sec. III E.

A popular view of the glass transition is the free-volume model of Cohen and Turnbull, based on the concept that statistical fluctuations in the liquid open up voids large enough for diffusive motion to occur.[34] Using the concept of

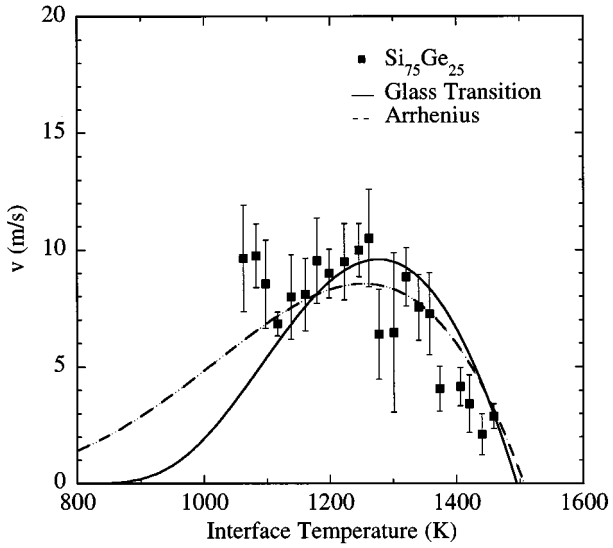

FIG. 5. The simulation results of the solidification velocity as a function of interface temperature for a $Si_{75}Ge_{25}$ alloy compared to the CGM without solute drag and using a short-range diffusion-limited growth model. The CGM predictions using the diffusion coefficient predicted by the glass transition and Arrhenius forms are indicated in solid and dashed lines, respectively.

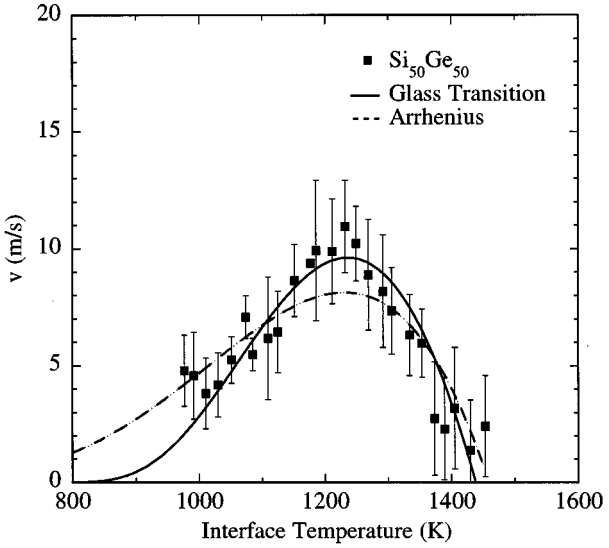

FIG. 6. The simulation results of the solidification velocity as a function of interface temperature for a $Si_{50}Ge_{50}$ alloy compared to the CGM without solute drag and using a short-range diffusion-limited growth model. Key as for Fig. 5.

free volume, one possible amorphization path is a simple kinetic quenching of the liquid. Although we do not know the congruent melting temperatures for amorphous SiGe alloys, the 470 K undercooling observed for the 75 at. % Ge alloy simulated here may be large enough to cause amorphization. As we see in Fig. 4 for the $T=860$ K run, once the interface has reached a peak velocity of 14 m/s, the growth slows with increasing undercooling and some solid remains uncrystallized at the thickness indicated in Fig. 3. Analysis of this solid using diffusion coefficient and structure factor data showed that this region is not a liquid, but a noncrystalline ''frozen solid'' with short-range order, i.e., a glass.

Similar plots to Figs. 3 and 4 were obtained for the other compositions studied. Each simulation that exhibited a steady-state recrystallization gave information allowing the construction of the interface response function. By lowering the substrate temperature, the steady-state interface temperature decreased, allowing more of the interface response function to be determined from one run. So, with a judicious choice of substrate temperature, the whole of the ''front side'' of the interface response function can be determined from only one run. Unfortunately, since we do not know how to choose appropriate substrate temperature for different alloys, we performed the simulations at a number of different substrate temperatures. This did, however, have the effect of improving the statistics for the interface response function. The simulation results of the interface response function, i.e., the solidification velocity versus interface temperature, averaged over numerous runs for 25, 50, and 75 at. % of Ge alloys are plotted in Figs. 5–7.

C. Effect of system size

In order to test system size effects, we increased the simulation cell from 5 to 7 unit cells in the X and Y directions and from 10 to 14 unit cells in the Z direction. This increased the system size from 2000 atoms to 5488 atoms. We performed simulations with this larger system size for a 25 at. % Ge alloy at a substrate temperature of 1187 K, a 50 at. % Ge alloy at 1111 K and a 75 at. % Ge alloy at 1010 K.

The results of the large system size for the 25 at. % Ge alloy are shown in Fig. 8. The solid-liquid interface moved very smoothly, as shown from the melt depth-time curve. The interface temperature also showed little fluctuation in the steady-state region. Steady-state regrowth was established immediately after passing the maximum melt depth. The partition coefficient during solidification was also better behaved than that in the small system shown in Fig. 1. Com-

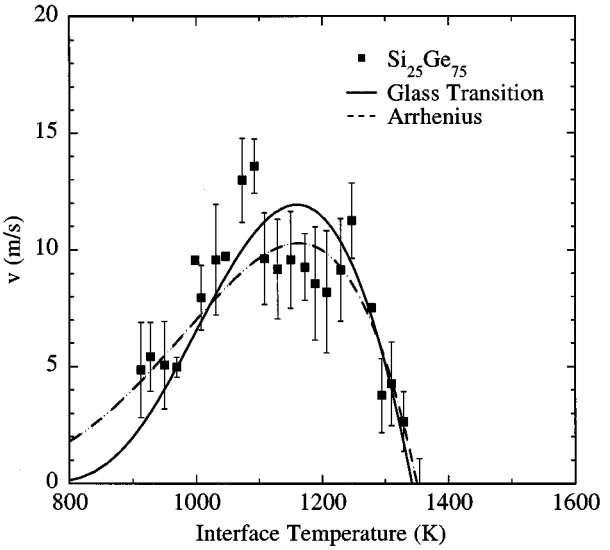

FIG. 7. The simulation results of the solidification velocity as a function of interface temperature for a $Si_{25}Ge_{75}$ alloy compared to the CGM without solute drag and using a short-range diffusion-limited growth model. Key as for Fig. 5.

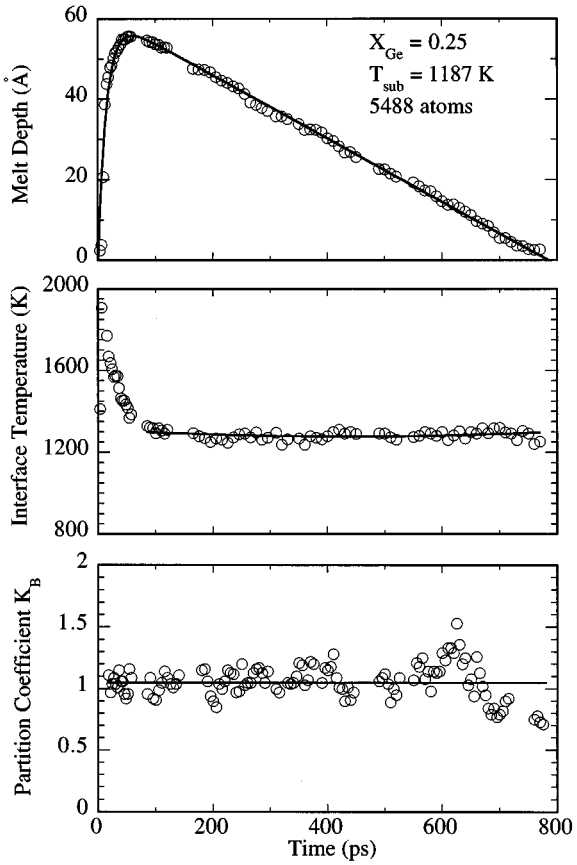

FIG. 8. Histories of the melt depth, interface temperature, and partition coefficient k_B of a nonequilibrium molecular-dynamics simulation of melting and rapid solidification for a $Si_{75}Ge_{25}$ alloy with 5488 atoms at a substrate temperature of 1187 K. Circles indicate raw data; lines represent the best fit to the data.

plete trapping of Ge in Si occurred for this system, as shown in Fig. 8. The solidification velocities differed by only 1 m/s between the two system sizes (see Table II). One would expect a somewhat lower interface velocity at the higher interface temperature of the larger system. However, this difference (1 m/s) is small compared to the strong system size dependence of growth velocity for the (111) orientation of LJ atoms found in the MD simulations by Burke *et al.*[35] In that case, changing the system size from 1200 to 4800 atoms decreased the velocity by about 10 m/s. Similar results were obtained for the 75 at. % Ge alloy, as shown in Fig. 9. In general, the solidification process described by the SW model is much better behaved than for the embedded atom method[27] (EAM) and LJ (Ref. 24) potentials. The large system size gives much better statistics but does not change the overall conclusions.

D. Maximum solidification velocity

As shown in Fig. 5 for a 25 at. % Ge alloy, the solidification velocity increases with undercooling of the interface until it reaches a maximum velocity. As shown in Table II, the interface velocities do not change very much over an interface temperature range of about 240 K. From these data, we consider that the maximum velocity in a 25 at. % Ge alloy is 9.0±0.5 m/s. Results for a 50 at. % Ge alloy (Fig. 6),

TABLE II. Maximum regrowth velocities v_{max} as a function of composition. T_{sub} is the substrate temperature at which the NEMD simulations were performed. T_{inter} and ΔT are, respectively, the solid/liquid interface temperature and interface undercooling where the maximum regrowth velocity is reached.

X_{Ge}	T_{sub} (K)	T_{inter} (K)	ΔT (K)	v_{max} (m/s)
0	1263	1316±43	266	20.2
0.05	1238	1306±45	334	18.1
0.25	1263	1340±7	224	8.8
0.25	1187	1255±10	309	8.9
0.25[a]	1187	1283±7	281	7.9
0.25	1086	1176±56	388	8.6
0.25	1010	1098±25	466	9.5
0.5	1187	1293±33	153	8.0
0.5	1111	1228±9	218	10.8
0.5	935	935	511	Amorphization
0.75	1086	1131±14	198	9.1
0.75	1010	1137±19	192	8.5
0.75	860	860	470	Amorphization
0.95	860	963±40	271	9.0
1.0	860	941±35	269	11.4

[a]Large system of 5488 atoms with 7×7×14 unit cells in X, Y, and Z directions.

shown in Table II, also allowed us to determine the maximum velocity for this alloy. However, if the substrate temperature is lowered to 935 K, solidification followed the ''back side'' unstable growth kinetics and the solidification velocity decreased gradually with decreasing interface temperature. So the maximum crystallization velocity is about 10.8 m/s for the 50 at. % Ge alloy. In Fig. 7 and Table II, the same phenomenon was observed for a 75 at. % Ge alloy. Again, lowering the substrate temperature to 860 K, as discussed in Sec. III B appeared to produce amorphization involving a glass transition, hence no points from this simulation are plotted on this figure. Therefore, the peak velocity of 14 m/s observed during this process (and shown in Figs. 3 and 4) could not be considered as a maximum *crystallization* velocity for this 75 at. % Ge alloy. It is more appropriate to use a maximum *crystal* regrowth velocity of ~9.0 m/s for this alloy. Simulations for 5 and 95 at. % Ge alloys as well as pure Ge and Si allowed the maximum crystallization velocities for these materials to be obtained in a similar manner.

The maximum regrowth velocity determined for the different alloys are plotted in Fig. 10. Unexpectedly, the maximum crystallization velocities of both Si-rich and Ge-rich alloys were found to decrease compared to those for pure Si and Ge. In order to check this prediction, we also measured the maximum crystallization velocity of liquid SiGe alloys experimentally (as well as liquid Si and Ge) during lateral and vertical explosive crystallization of amorphous SiGe alloys, Si and Ge.[36] Interestingly, the same trend is obtained in the experiments (Fig. 10).

E. Diffusion coefficient

In the short-range diffusion-limited growth rate theory, the solidification velocity is controlled by the mobility of

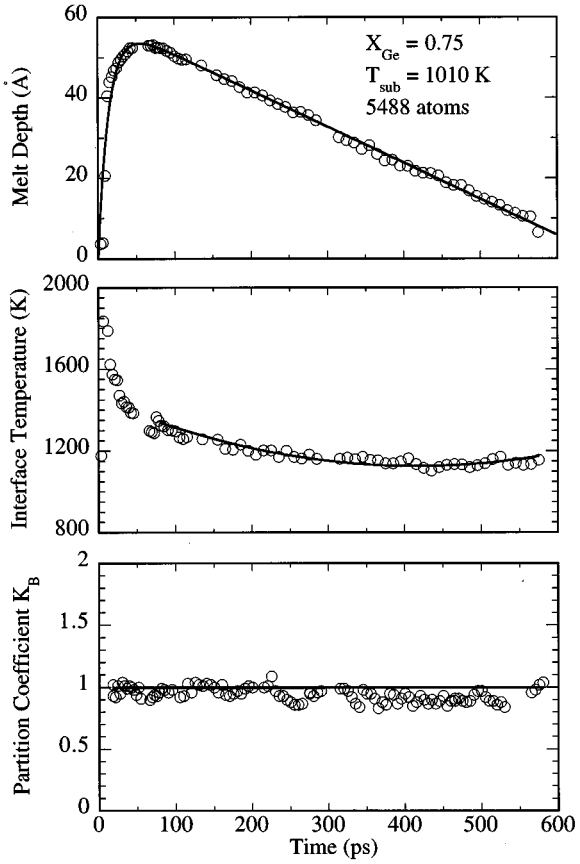

FIG. 9. Histories of the melt depth, interface temperature, and partition coefficient k_B of a nonequilibrium molecular-dynamics simulation of melting and rapid solidification for a $Si_{25}Ge_{75}$ alloy with 5488 atoms at a substrate temperature of 1010 K. Key as for Fig. 8.

atoms in the liquid, so it is important to understand the diffusion behavior of each component in the alloy. In the experiments, however, only the bulk liquid diffusion coefficient of Ge near the melting point can be extracted by analysis of results from laser-induced rapid solidification[15,16,37] or from the solute segregation studies.[38] On the other hand, it is straightforward to obtain the bulk liquid diffusion coefficients of both Si and Ge at different temperatures in MD simulations. These data can be used to obtain the activation energy and prefactor D_0 in an Arrhenius equation for the diffusion coefficient in the liquid phase:

$$D(T)=D_0\exp\left(\frac{-E_d}{kT}\right), \tag{7}$$

where E_d is the activation energy of the diffusion coefficient, D_0 is the prefactor, and k is Boltzmann's constant. Grabow *et al.*[9] have estimated the temperature dependence of the diffusion coefficient for pure Si modeled by SW potentials using MD simulations. The diffusion expression was determined to be Arrhenius-like with $D_0=3.5\times10^{-3}$ cm^2/s and $E_d=0.56$ eV. This leads to $D(T_m)=7.5\times10^{-5}$ cm^2/s, which is one-third the experimental value of $D(T_m)\approx2\times10^{-4}$ cm^2/s.[39] A similar value of 6.94×10^{-5} cm^2/s for pure Si was found also in MD simulations using SW potentials.[33]

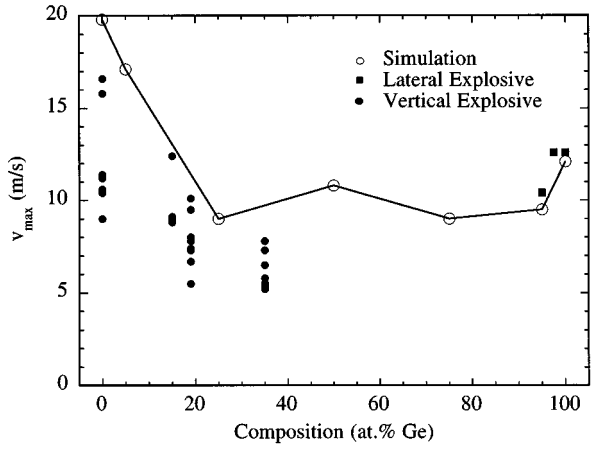

FIG. 10. The maximum crystallization velocity as a function of Ge composition from NEMD simulation (open circle), lateral (filled square), and vertical (filled circle) explosive crystallization measurements. The solid line is intended as a guide to the eye through the simulation results.

Liquid phase diffusion coefficients can be measured until the glass transition occurs. There is now some consensus as to the temperature at which this occurs, quoted earlier in Sec. III B. In systems for which a glass transition exists, the Vogel-Fulcher form of the diffusion coefficient is[40,41]

$$D(T)=D_0\exp\left[\frac{-E_d}{k(T-T_g)}\right], \tag{8}$$

where T_g is the glass transition temperature. Instead of a linear relationship between the logarithm of D and reciprocal temperature given by the Arrhenius form, the characteristic of this relationship is a convex curve. The higher the glass transition temperature, the more apparent the curvature. We will use both these forms to try to fit the diffusion coefficients and the interface response function for the alloys.

The diffusion coefficients of Si and Ge in bulk liquid were calculated using constant volume-constant temperature (NVT) MD simulations. At a given temperature, the diffusion coefficient was calculated from the slope of the mean-squared displacement as a function of time. The mean-squared displacement was averaged for 40 ps with averages calculated over 100 time origins to reduce statistical error. The results for the diffusion coefficient of Si and Ge in the 25 at. % Ge alloy as a function of temperature are shown in Figs. 11 and 12, respectively. It is apparent that the curves are convex and fit the glass transition form for the diffusion coefficient rather than Arrhenius form. The same behavior is observed for the other alloy systems studied. Values of the activation energy E_d, the prefactor D_0, and the glass transition temperature T_g fitted to the glass transition form are listed in Table III. The diffusion coefficients fitted to the Arrhenius form and the resulting D_0 and E_d values are also listed in Table III. As we can see, a glass transition does exist in the SiGe alloys. In general, the glass transition temperature and prefactor decrease as the Ge composition in the alloy increases. In Arrhenius form, the activation energy and prefactor increase with increasing Ge composition for Si, but

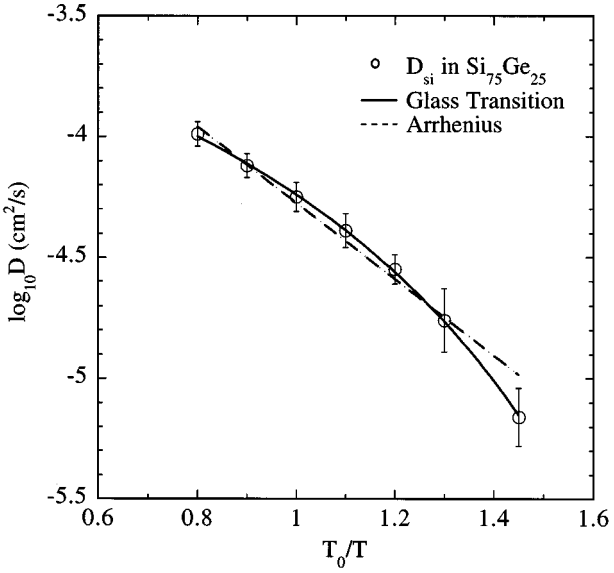

FIG. 11. Diffusion coefficients of Si in a $Si_{75}Ge_{25}$ alloy as a function of the reciprocal temperature. Open circles are the molecular-dynamics results; solid line represents the fit given by the glass transition form; the dashed line is a fit to the Arrhenius form.

are almost unchanged for Ge. The activation energy in the glass transition form varies within 0.03 eV in different SiGe alloys.

If we apply the same procedure for the diffusion coefficient of pure Si, the temperature dependence of the diffusion coefficient is almost a linear relationship with very weak convex curvature. The glass transition temperature for pure Si is only 247 K if fitted to the glass transition form, in sharp contrast to the direct simulation results and experiments quoted earlier.[30–33] We refitted the temperature dependence of the liquid diffusivity and growth rates for SW Si obtained by Grabow *et al.*[9] and obtained an estimate of a glass transition temperature of 420–500 K.

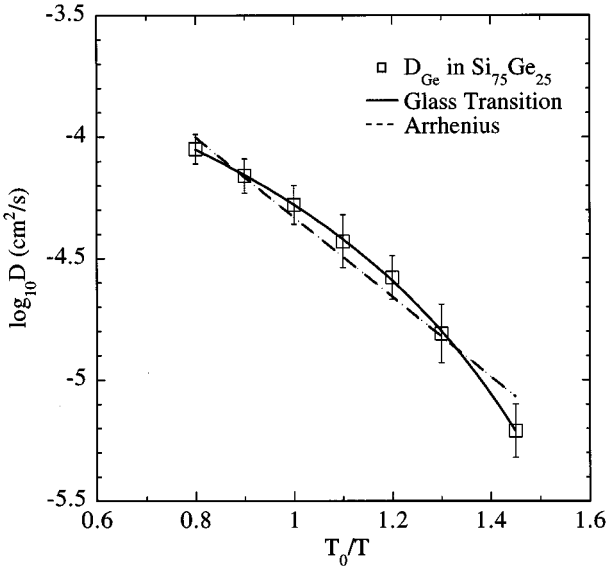

FIG. 12. Diffusion coefficients of Ge in a $Si_{75}Ge_{25}$ alloy as a function of the reciprocal temperature. Key as for Fig. 11.

TABLE III. The activation energy of diffusion E_d (eV), the prefactor D_0 ($\times 10^{-4}$ cm^2/s), and glass transition temperature T_g (K), fitted to the glass transition diffusion coefficient form and the Arrhenius form for Si and Ge in different $Si_{1-x}Ge_x$ alloys.

	Si			Ge		
X_{Ge}	D_0	E_d	T_g	D_0	E_d	T_g
			Glass transition form			
0.05	3.6	0.14	741	4.0	0.15	726
0.25	3.7	0.15	653	2.8	0.13	703
0.50	3.2	0.13	671	3.7	0.16	614
0.75	2.9	0.14	607	3.2	0.15	577
0.95	2.1	0.11	617	2.8	0.13	556
			Arrhenius form			
0.05	17.2	0.49		37.9	0.60	
0.25	20.1	0.49		20.4	0.51	
0.50	31.1	0.55		44.3	0.59	
0.75	50.5	0.60		43.2	0.58	
0.95	91.5	0.65		35.0	0.53	

The diffusion coefficients of Si and Ge at the congruent melting temperature of each alloy were estimated from the glass transition form and are listed in Table IV. The diffusion coefficients of Si and Ge in the Si-rich alloys are about 2–3 times higher than those in the Ge-rich alloys from both the glass transition form and the Arrhenius form. Similar phenomena were also observed by Romanenko and Smirnov[38] in a study of solute segregation in Czochralski-grown crystals. The diffusivities near the crystallization temperature for both Si and Ge in liquid $Si_{1-x}Ge_x$ were extracted from this study. The diffusion coefficient for Ge is 6×10^{-4} cm^2/s in nearly pure liquid Si. It falls to 4.5×10^{-4} cm^2/s at 10 at. % Ge and 1.5×10^{-4} cm^2/s at 30 at. % Ge, a stronger composition dependence of the Ge diffusion coefficient than we observed in MD simulations. They also calculated diffusion coefficients based on the Einstein-Stokes equation. No composition dependence of the diffusion coefficients was found from this calculation. This lack of composition dependence could be due to the neglect of the temperature dependence of the dy-

TABLE IV. The diffusion coefficients of Si and Ge at the congruent melting temperature of each alloy.

X_{Ge}	D_{Si} ($\times 10^{-5}$ cm^2/s)	D_{Ge} ($\times 10^{-5}$ cm^2/s)
	Glass transition form	
0.05	6.1	6.4
0.25	5.6	5.2
0.50	4.8	4.5
0.75	3.0	3.3
0.95	2.3	3.0
	Arrhenius form	
0.05	5.7	5.8
0.25	5.4	4.7
0.50	3.8	4.0
0.75	2.7	2.8
0.95	2.0	2.4

namic viscosity in their calculations. On the other hand, recent experiments by Brunco *et al.*[15] of the diffusion coefficients of Ge in liquid $Si_{1-x}Ge_x$ alloys during pulsed laser annealing showed no obvious concentration dependence for Ge compositions up to 10 at. %. As the temperature of the melting front varies with Ge concentration, so also does the real temperature at the interface vary with the crystallization velocity. Given the scatter of the diffusivity data and temperatures close to the Si melting temperature, it is not clear that any composition dependence of the diffusivity of Ge is observable in their experiments.

The Ge diffusion coefficient in $Si_{1-x}Ge_x$ alloys for Ge compositions less than 10 at. % are $2.5–6\times10^{-4}$ cm^2/s, as measured in several experiments.[15,16,37,38] The diffusion coefficient of Ge calculated from our MD simulation is 6.4×10^{-5} cm^2/s in a 5 at. % Ge alloy, which is lower by a factor of 4–10 than the experimental values. MD simulations by Grabow *et al.*[9] and Broughton and Li[33] also underestimated the diffusion coefficient for Si using SW potentials. Hence, this difference appears to be the result of deficiencies in the SW potential.

F. Comparison to CGM theory

First, the CGM without solute drag[1] was tested for its ability to describe the relationship of solidification velocity and interface temperature for SiGe alloys using the NEMD simulation results. This involves solving Eq. (1) with the prefactor v_0 calculated from Eq. (2) and a suitable expression for $\Delta\mu$. In the CGM without solute drag, combined with regular solution theory to calculate the Gibbs free energy $\Delta\mu$ is represented by

$$\begin{aligned}\Delta\mu(T_i,X_s,X_l)&=\Delta G_{\mathrm{DF}}=X_s\Delta\mu_B+(1-X_s)\Delta\mu_A\\&=\Delta H^A\left(\frac{T_m^A-T_i}{T_m^A}\right)(1-X_S)\\&\quad+\Delta H^B\left(\frac{T_m^B-T_i}{T_m^B}\right)X_S+\Omega_s[X_s^2(1-X_s)\\&\quad+(1-X_s)^2X_s]-\Omega_l[X_l^2(1-X_s)\\&\quad+(1-X_l)^2X_s]+RT_i\left[(1-X_s)\ln\left(\frac{1-X_s}{1-X_l}\right)\right.\\&\quad\left.+X_s\ln\left(\frac{X_s}{X_l}\right)\right],\end{aligned}\tag{9}$$

where ΔH^B and ΔH^A represent changes in enthalpy on solidification, for solute and solvent, T_m^B and T_m^A the equilibrium melting temperature for solute and solvent, and Ω_s and Ω_l the interaction parameter for solid and liquid. Since the simulation results are being compared with CGM, all the parameters in the calculation are used from simulation. The latent heat for Si obtained from the SW potential was used in the calculation of the Gibbs free energy, although it is known to be only about 60% of the experimental value.[33] The latent heat for Ge was scaled by the ratio of the energy parameters for Ge and Si used in this simulation, i.e., 0.71, as given in Sec. II. The solute composition in the solid at the solid-liquid interface is fixed. To simplify the problem, the partition coefficient was first set equal to unity for all velocities, even though it is known to vary from the equilibrium value at zero velocity to a value of unity at high velocities. The interaction parameter Ω_s was allowed to vary. According to the *quasichemical* approach, Ω is given by

$$\Omega=N_a z\epsilon,\tag{10}$$

where N_a is Avogadro's number, z is the number of bonds per atom, and ϵ is the difference between the A-B bond energy and the average of the A-A and B-B bond energies, which is

$$\epsilon=\epsilon_{AB}-\tfrac{1}{2}(\epsilon_{AA}+\epsilon_{BB}).\tag{11}$$

It is known from MD simulations of SW Si that the number of bonds per atom are 4 in the solid and approximately 6.2 in the liquid.[33] So, Ω_s is varied in the fitting and $\Omega_l=6.2/4.0\Omega_s$.

The short-range diffusion-limited theory was used for the kinetic prefactor, as presented in Eq. (2). Diffusion coefficients of Si and Ge in the SiGe alloys obtained in MD simulations were used. The distance between atomic layers in the (100) direction, d, is equal to 1.3575 Å for Si and 1.4145 Å for Ge. For SiGe alloys, this distance scales linearly with Ge composition. The mean free path in the liquid, λ, is given by $\lambda=mr_0$, where m is a constant and r_0 is the nearest-neighbor spacing and is 2.35 Å for Si. Also, λ for the alloys scales linearly with Ge composition. The constant m was determined to be about 0.1–0.4 for pure Si.[9] Here, this constant m and f are combined into a new adjustable variable, m'.

The solidification velocity versus interface temperature calculated from the CGM without solute drag and with a short-range diffusion-limited kinetic prefactor for 25, 50, and 75 at. % Ge alloys are shown in Figs. 5–7. The diffusion coefficients in the glass transition form and Arrhenius form were used in the calculation of v versus T_i. In general, a steeper front side and back side of the interface response function is predicted by the glass transition form of diffusion coefficient than the Arrhenius form. Due to the scatter in the simulation data, it is not possible for us to say which form of the diffusion coefficient gives a better representative of the interface velocity-temperature response function. The two fitted variables Ω_s and m' are listed in Table V.

TABLE V. Values of Ω_s and m' for SiGe alloys fitted to the CGM without solute drag and using the short-range diffusion-limited kinetic prefactor with the diffusion coefficient in the glass transition and Arrhenius forms.

X_{Ge}	T_g (K)	Ω_s (K J/mol)	m'	T_g (K)	Ω_s (K J/mol)	m'
0.25	703 (Ge)	−11.16	5.68	0	−9.38	5.50
0.50	670 (Si)	−0.84	6.10	0	1.74	5.67
0.75	607 (Si)	2.47	10.99	0	3.78	11.22

Since the partition coefficient is assumed to be unity, the temperature at zero solidification velocity is the congruent melting temperature. Note that the interaction parameter Ω_s varied from negative to positive values in order to fit the simulation results, reflecting the differing quality of prediction of the congruent melting temperature by the simulations.

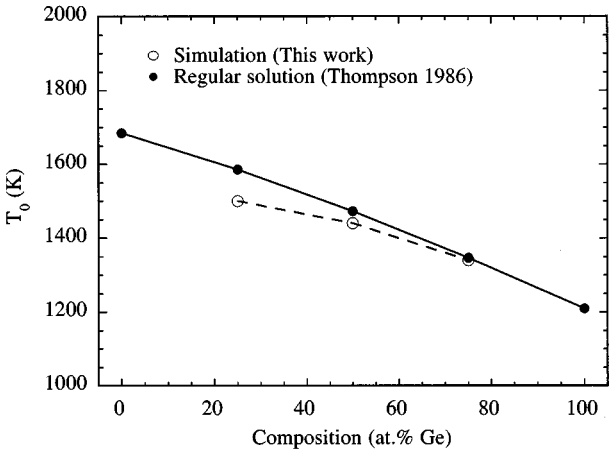

FIG. 13. The congruent melting temperature for SiGe alloys obtained from simulations and calculations (Ref. 25).

The congruent melting temperatures for SiGe alloys obtained from the simulation are compared in Fig. 13 with those calculated by assuming a partitionless melt and solidification and a regular solution.[25] The values of the interaction parameters, Ω, for solid and liquid phases are -3.5 K J/mol and -6.5 K J/mol, respectively,[42] obtained by fitting to the experimental phase diagram.

Now, let us consider the effect on the results if the partition coefficient is allowed to vary with the solidification velocity, with $k_e=0.45$ and $v_D=2$ m/s.[21] For solidification velocities faster than 4 m/s, there was no apparent effect on the results. Under 4 m/s, more undercooling is predicted if k_B is allowed to vary with velocity, due to the partitioning of the solute at the solid-liquid interface. This effect, however, is very weak, changing the undercooling by <10 K in all cases. The partition coefficient dependence of the solidification velocity using the form of CGM developed for concentrated solutions was also used to solve the interface velocity and undercooling equations. No difference in the results was observed using the forms for dilute solution and for concentrated solution, which is consistent with the recent results of Aziz and Boettinger.[12] We also tested the CGM with solute drag included. As noted in Eqs. (4) and (5), CGM theory with and without solute drag has the same expression at fast regrowth region where the partition coefficient approaches unity and the solute concentration in the solid X_s and in the liquid X_l at the interface are the same. To distinguish the solidification behavior of SiGe alloys using CGM with and without solute drag required us to study the slow regrowth region. However, we found that the predicted solute drag effect using CGM with solute drag is negligibly small compared to the scatter in simulation data. This is not surprising since SiGe alloys form almost ideal solutions. Recently, a direct measurement of velocity-interface temperature data on nonideal solutions of Si-As alloys tested the CGM theory with and without solute drag and showed the absence of solute drag in solidification.[17–19]

IV. CONCLUSIONS

Significant mutual solute trapping of Ge as an impurity in Si and Si as an impurity in Ge, was found at high solidification velocities, which confirmed the predictions of the CGM and experimental measurements.[16] The solidification velocity as a function of interface temperature for different composition SiGe alloys showed the maximum regrowth velocity to be remarkably consistent from run to run. The maximum crystallization velocity found for each alloy corresponded to an approximately 20% undercooling of the interface. Configurational ''freezing'' of the liquid during the rapid solidification of SiGe alloys was observed in simulations at very low substrate temperatures. During this process, an amorphization appears to have taken place. Studies using CGM and a short-range diffusion-limited growth model were tested as a description of the relationship between solidification velocity and interface temperature. The variation of the partition coefficient with interface velocity given by CGM for dilute and concentrated solutions gave similar results. Impurity partitioning results in a need for more undercooling to reach the same solidification velocity. An unexpectedly nonlinear relationship of maximum crystallization velocity and Ge composition was found both in simulation and experiment. The maximum crystallization velocity of SiGe alloys was less than those for both pure components.

ACKNOWLEDGMENTS

The authors would like to thank the Semiconductor Research Corporation (Grant No. 93-SC-069) and the National Science Foundation (Grant No. DMR-8915333) for financial support of this work. We would also like to thank Digital Equipment Corporation for providing a high performance DEC 3000-500 workstation on which most of these simulations were performed. David P. Brunco is thanked for helpful discussions.

*Current address: Center for Space Microelectronics Technology, Jet Propulsion Laboratory, California Institute of Technology, Pasadena, CA 91109.

†Author to whom correspondence should be addressed.

[1] M. J. Aziz and J. Kaplan, Acta Metall. **36**, 2335 (1988).

[2] K. A. Jackson, G. H. Gilmer, and H. J. Leamy, in *Laser and Electron Beam Processing of Materials*, edited by C. W. White and P. S. Peercy (Academic, New York, 1980), pp. 104–110.

[3] K. A. Jackson, in *Surface Modification and Alloying by Laser, Ion and Electron Beams*, edited by J. M. Poate, G. Foti, and D. C. Jacobson (Plenum, New York, 1983), p. 51.

[4] H. A. Wilson, Proc. Cambridge Phil. Soc. **10**, 25 (1898); Philos. Mag. **50**, 238 (1900).

[5] J. Frenkel, Phys. Z. Sowjetunion **1**, 498 (1932).

[6] K. A. Jackson, in *Treatise on Solid State Chemistry*, edited by N. B. Hannay (Plenum, New York, 1975), Vol. 5, pp. 233-282.

[7] K. A. Jackson and B. Chalmers, Can. J. Phys. **34**, 473 (1956).

[8] P. A. Stolk, A. Polman, and W. C. Sinke, Phys. Rev. B **47**, 5 (1993).

[9] M. H. Grabow, G. H. Gilmer, and A. F. Bakker, in *Atomic Scale Calculations in Materials Science*, edited by J. Tersoff, D. Vanderbilt, and V. Vitek, MRS Symposia Proceedings No. 141

(Materials Research Society, Pittsburgh, 1989), p. 349.
[10] D. Turnbull, J. Phys. Chem. **66**, 609 (1962).
[11] J. Y. Tsao, M. J. Aziz, M. O. Thompson, and P. S. Peercy, Phys. Rev. Lett. **56**, 2712 (1986).
[12] M. J. Aziz and W. J. Boettinger, Acta Metall. **42**, 527 (1994).
[13] K. Eckler, D. M. Herlach, and M. J. Aziz, Acta Metall. **42**, 975 (1994).
[14] P. M. Smith and M. J. Aziz, Acta Metall. Mater. **42**, 3515 (1994).
[15] D. P. Brunco, M. O. Thompson, D. E. Hoglund, M. J. Aziz, and H.-J. Gossmann, J. Appl. Phys. **78**, 1575 (1995).
[16] M. J. Aziz, J. Y. Tsao, M. O. Thompson, P. S. Peercy, C. W. White, and W. H. Christie, in *Energy Beam-Solid Interactions and Transient Thermal Processing*, edited by D. K. Biegelsen, G. A. Rozgonyi, and C. V. Shank, MRS Symposia Proceedings No. 35 (Materials Research Society, Pittsburgh, 1985), p. 153.
[17] J. A. Kittl, M. J. Aziz, D. P. Brunco, and M. O. Thompson, Appl. Phys. Lett. **64**, 2359 (1994).
[18] J. A. Kittl, R. Reitano, M. J. Aziz, D. P. Brunco, and M. O. Thompson, J. Appl. Phys. **73**, 3725 (1993).
[19] J. A. Kittl, M. J. Aziz, D. P. Brunco, and M. O. Thompson, J. Cryst. Growth **148**, 172 (1995).
[20] F. H. Stillinger and T. A. Weber, Phys. Rev. B **31**, 5262 (1985).
[21] Q. Yu and P. Clancy, J. Cryst. Growth **149**, 45 (1995).
[22] Q. Yu and P. Clancy, Modeling Simul. Mater. Sci. Eng. **2**, 829 (1994).
[23] D. K. Chokappa, S. J. Cook, and P. Clancy, Phys. Rev. B **39**, 10 075 (1989).
[24] S. J. Cook and P. Clancy, J. Chem. Phys. **99**, 2175 (1993); **99**, 2192 (1993).
[25] M. O. Thompson, P. S. Peercy, J. Y. Tsao, and M. J. Aziz, Appl. Phys. Lett. **49**, 558 (1986).
[26] M. J. Uttormark, S. J. Cook, M. O. Thompson, and P. Clancy, in *Kinetics of Phase Transformations*, edited by M. O. Thompson, M. Aziz, and G. B. Stephenson, MRS Symposia Proceedings No. 205 (Materials Research Society, Pittsburgh, 1992), p. 417.
[27] C. F. Richardson and P. Clancy, Mol. Sim. **7**, 335 (1991).
[28] J. A. Yater, Ph.D. Thesis, Cornell University, 1992.
[29] M. Von Allmen, in *Beam-Solid Interactions and Transient Thermal Processing of Materials*, edited by J. Narayan, W. L. Brown, and R. A. Lemons, MRS Symposia Proceedings No. 12 (Materials Research Society, Pittsburgh, 1983), p. 691.
[30] P. E. Evans and S. R. Stiffler, Acta Metall. **39**, 2727 (1991).
[31] A. P. Horsfield and P. Clancy, Modeling Simul. Mater. Sci. Eng. **2**, 277 (1994).
[32] S. J. Cook and P. Clancy, Phys. Rev. B **47**, 7686 (1994).
[33] J. Q. Broughton and X. P. Li, Phys. Rev. B **35**, 9120 (1987).
[34] M. H. Cohen and D. Turnbull, J. Chem. Phys. **31**, 1164 (1959).
[35] E. Burke, J. Q. Broughton, and G. H. Gilmer, J. Chem. Phys. **89**, 1030 (1988).
[36] Q. Yu, K. Kramer, D. P. Brunco, P. Clancy, and M. O. Thompson (unpublished).
[37] R. Reitano, P. M. Smith, and M. J. Aziz, J. Appl. Phys. **76**, 1518 (1994).
[38] V. N. Romanenko and Yu. M. Smirnov, Inorg. Mater. (USSR) **6**, 1527 (1970).
[39] P. Baeri, S. U. Campisano, G. Foti, and E. Rimini, Phys. Rev. Lett. **41**, 1246 (1978).
[40] G. S. Fulcher, J. Am. Ceram. Soc. **6**, 339 (1925).
[41] H. Vogel, Phys. Z. **22**, 645 (1921).
[42] R. W. Olesinski and G. J. Abbaschian, Bull. Alloy Phase Diagram **5**, 180 (1984).